

## Article

# Trace Elements of Gangue Minerals from the Banbianjie Ge-Zn Deposit in Guizhou Province, SW China

Yun-Lin An <sup>1,2</sup>, Jia-Xi Zhou <sup>1,3,4,\*</sup> , Qing-Tian Meng <sup>5</sup>, Guo-Tao Sun <sup>6</sup> and Zhi-Mou Yang <sup>1,2</sup>

<sup>1</sup> Key Laboratory of Critical Minerals Metallogeny in Universities of Yunnan Province, School of Earth Sciences, Yunnan University, Kunming 650500, China

<sup>2</sup> Zijin Mining Group Co., Ltd., Longyan 364200, China

<sup>3</sup> Key Laboratory of Sanjiang Metallogeny and Resources Exploration & Utilization, MNR, School of Earth Sciences, Yunnan University, Kunming 650500, China

<sup>4</sup> Yunnan Key Laboratory of Sanjiang Metallogeny and Resources Exploration & Utilization, School of Earth Sciences, Yunnan University, Kunming 650500, China

<sup>5</sup> No. 104 Geological Team, Guizhou Bureau of Geology and Mineral Exploration and Development, Duyun 558000, China

<sup>6</sup> College of Resources and Environmental Engineering, Guizhou University, Guiyang 550025, China

\* Correspondence: zhoujiaxi@ynu.edu.cn

**Abstract:** There are many dispersed element-rich Pb-Zn deposits hosted by Paleozoic carbonate rocks in the Middle-Upper Yangtze Block, China. The origin and nature of the ore-forming fluids that formed them are still much debated (syngenetic vs. epigenetic). The Banbianjie Ge-Zn deposit is located in the southeastern margin of the Yangtze Block, SW China. It is a newly discovered medium-sized Zn (Zn metal reserves > 0.39 Mt, @1.78%–9.5% Zn) and large-scale Ge deposit (Ge metal resources > 900 t, @ $100 \times 10^{-6}$ – $110 \times 10^{-6}$  Ge) in the Western Hunan–Eastern Guizhou Pb-Zn metallogenic belt, SW China. Gangue minerals in the Banbianjie deposit are very developed, including calcite, dolomite and barite, which are closely associated with sulfides. Hence, the trace elements of gangue minerals could be used to trace the nature, source and evolution of ore-forming fluids, and the ore genesis of this deposit can be discussed. These gangue minerals are nearly horizontally distributed in the plot of La/Ho–Y/Ho, suggesting that they are the products of the same hydrothermal fluids. The total rare earth element ( $\Sigma$ REE) contents from calcite and dolomite to barite show an increasing trend, indicating that the REEs in the ore-forming fluids were mainly enriched in barite. Hence, the  $\Sigma$ REE of barite can approximately represent the  $\Sigma$ REE of the hydrothermal fluids, which are quite similar to those of the underlying strata, indicating that the ore-forming fluids were likely originated from and/or flowed through them. The Eu anomalies from dolomite (Eu/Eu\* = 0.33–0.66) to calcite (Eu/Eu\* = 0.29–1.13) and then to barite (Eu/Eu\* = 1.64–7.71) show an increasing trend, suggesting that the ore-forming fluids experienced a shift in the ore-forming environment from reduced to oxidized. Hence, the source of the Banbianjie Ge-Zn deposit is the underlying strata, and the ore-forming physical–chemical condition has experienced a transition from reduction to oxidation during the Ge-Zn mineralization. The ore genesis of the Banbianjie Ge-Zn deposit is most likely a Mississippi Valley-type (MVT) deposit.

**Keywords:** Banbianjie Ge-Zn deposit; gangue minerals; nature; source and evolution of ore-forming fluids; trace elements; Western Hunan–Eastern Guizhou Pb-Zn metallogenic belt; SW China



**Citation:** An, Y.-L.; Zhou, J.-X.; Meng, Q.-T.; Sun, G.-T.; Yang, Z.-M. Trace Elements of Gangue Minerals from the Banbianjie Ge-Zn Deposit in Guizhou Province, SW China. *Minerals* **2023**, *13*, 638. <https://doi.org/10.3390/min13050638>

Academic Editor: Daniel Marshall

Received: 11 April 2023

Revised: 30 April 2023

Accepted: 2 May 2023

Published: 4 May 2023



**Copyright:** © 2023 by the authors. Licensee MDPI, Basel, Switzerland. This article is an open access article distributed under the terms and conditions of the Creative Commons Attribution (CC BY) license (<https://creativecommons.org/licenses/by/4.0/>).

## 1. Introduction

Dispersed metals (Ga, Ge, Se, Cd, In, Te, Re and Tl) are widely used in emerging industries and are critical metals [1–3]. Germanium, a typical dispersed metal, only has a CLARKE value of about  $1.5 \times 10^{-6}$  [1]. Industrial germanium mainly comes from lead–zinc mines and coal mines [2,3]. There are many Ge-rich Pb-Zn deposits hosted by Paleozoic

carbonate rocks in the Middle-Upper Yangtze Block, China [3–5]. The genesis of these Ge-rich Pb-Zn deposits has attracted widespread attention.

The study area is located in the southeastern margin of the Yangtze Block, SW China, which is an important part of the Western Hunan–Eastern Guizhou (WHEG) Pb-Zn metallogenic belt and contains many dispersed element-rich Pb-Zn deposits (such as Cd-rich Niujiatong and Ge-rich Zhulingou and Banbianjie) [4–8]. The distribution of these deposits is jointly controlled by the WE-trending Huangsi and NE-trending Mandong faults [9]. Previous studies have shown that the source of sulfur in these deposits is the marine sulfates within the ore-bearing strata, and the ore-forming metals (Zn, Ge, Cd, etc.) were mainly sourced from the basement rocks [10–14]. However, the nature and source of ore-forming fluids are still controversial: (i) ore-forming fluids are characterized by “multi-source” [11,15–19]; (ii) ore-forming fluids are associated with ancient oil and gas reservoirs [4,10]; (iii) stratigraphic fluids [20]; and (iv) deep circulation basin brine [6]. In addition, studies on the evolution of ore-forming fluids are rarely reported.

In our previous study, isotope geochemistry was used to trace the source of ore-forming elements (such as S and Pb) [14]. As the trace elements characteristics of hydrothermal minerals depend on the nature, composition and physical–chemical condition of ore-forming fluids [21–25], they are widely used to explore the nature, source and evolution of hydrothermal fluids. Based on the previously reported whole-rock rare earth elements (REE) of partial dolomite [14], this paper analyzed the in situ trace elements (including REE) of gangue minerals (dolomite, calcite and barite) from the Banbianjie Ge-Zn deposit to reveal this issue, which provided more abundant geochemical information for comprehending the ore genesis of the deposit.

## 2. Regional Geology Setting

The study area is located in the southeastern margin of the Yangtze Block and the western margin of the Jiangnan Orogenic Belt (Figure 1a). It is mainly confined by three regional deep faults: the Tongren–Sandu fault to the east, the Ziyun–Luodian fault to the south and the Guiyang–Zhenyuan fault to the north [26–28]. The regional strata include metamorphic basements and overlying sedimentary covers. Among them, the oldest stratigraphic unit is the Upper Proterozoic Banxi Group, which consists of metamorphic sandstone, slate and a small amount of carbonate rocks [29,30]. The Paleozoic–Cenozoic sedimentary strata are mainly composed of carbonate rocks, argillaceous sandstone and shales, and the spatial distribution has the characteristic of old to new from east to west (Figure 1b). The Cambrian–Devonian carbonate rocks are the main ore-bearing rocks for these dispersed element-rich Pb-Zn deposits [6,31,32].

Since the formation period of the Wuling–Jinning basement, the study area has successively experienced the tectonic evolution of the Xuefeng–Caledonian ocean–land transition, the Indosinian–Yanshanian orogeny and the Himalayan differential uplift. The main structures are folds, faults and thrust nappe structures [33–35]. The evolution of the fractured ocean basin is closely related to the formation of many endogenous hydrothermal metallic minerals (e.g., Au, Sb, Pb, Zn, Mn, Mo and Ni deposits) and sedimentary minerals resources (e.g., phosphate ores and shale gas) in this area [30]. The hydrothermal deposits are mainly structurally controlled by the NE-trending Mandong and near EW-trending Huangsi faults (Figure 1b).

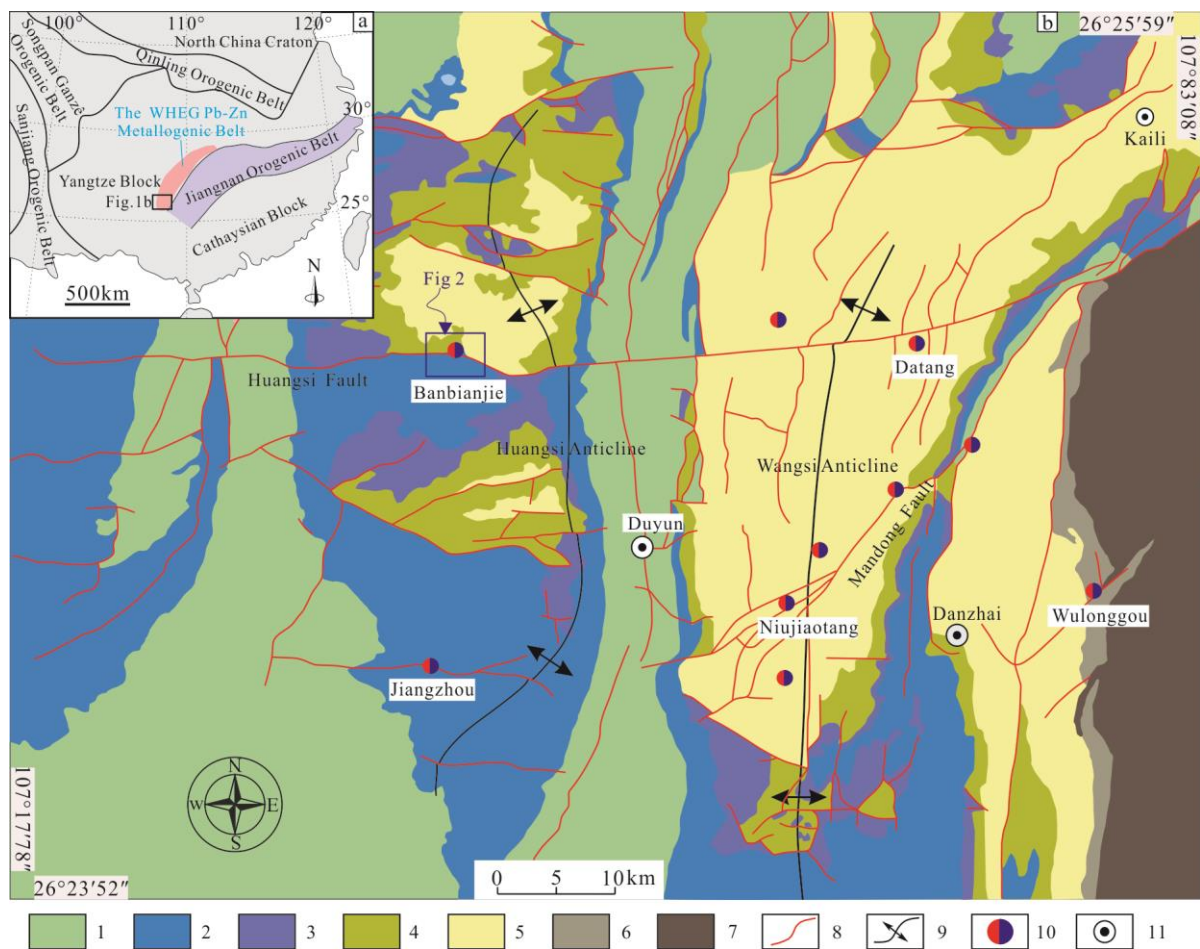


**Figure 1.** (a) Sketch map of the Western Hunan–Eastern Guizhou Pb–Zn metallogenic belt in the Yangtze Block (modified after [36]); (b) structural sketch map for the deposits in southern Guizhou district (modified after [37]). 1—Carboniferous–Permian sandstone and mudstone; 2—Devonian dolostone; 3—Silurian sandstone; 4—Ordovician limestone; 5—Cambrian dolostone; 6—Sinian dolomite and sandstone; 7—Banxi Group metamorphic rocks; 8—Fault; 9—Anticline; 10—Pb–Zn deposit; 11—City.

### 3. Geology of Ore Deposit

#### 3.1. Strata

The strata are Silurian, Devonian, Carboniferous, Permian and Quaternary from ancient to present (Figure 2). The Silurian to Middle Devonian consists of coastal clastic sedimentary rocks, the Upper Devonian is a set of confined marine mesa facies post-reef lagoon carbonate rocks, the Carboniferous to Permian is carbonate mesa facies sedimentary rocks and the Quaternary consists of residual and slope wash (Figure 2). The Upper Devonian can be further divided into three sections (Figure 3). The Upper Devonian Gaopochang Formation second section ( $D_3g^2$ ) is the main ore-bearing position of the Banbianjie Ge–Zn deposit, and its overall lithologies can be divided into three layers. The upper layer ( $D_3g^{2a}$ ) is dark-gray flint-bearing clumpy fine-grained dolostone, with black argillaceous bands and geodes interspersed, and fissure and dolomite veins are developed. The middle layer ( $D_3g^{2b}$ ) is dark-gray biotritus fine-grained dolostone, with gray-yellow argillaceous bands interspersed, and fractures are relatively developed, as well as clumpy and veined dolomites, which are messily distributed. The lower layer ( $D_3g^{2c}$ ) is light-gray medium-thickness siliceous fine-grained dolostone, with gray-yellow argillaceous bands interspersed (Figure 2). The ore-bearing rocks are the argillaceous bands dolostone.

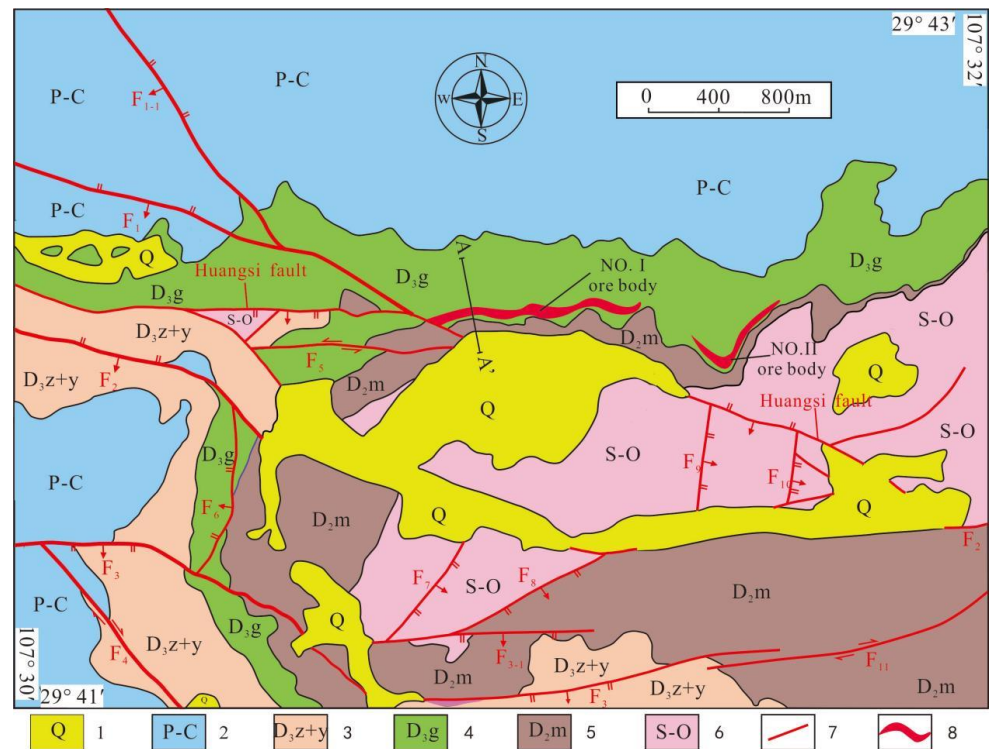


**Figure 2.** Sketch geological map of the Banbianjie mining area, Guizhou province (modified after [13]). 1—Quaternary; 2—Permian-Carboniferous; 3—Upper Devonian Zhewang and Yaosuo Formations; 4—Upper Devonian Gaopochang Formation; 5—Middle Devonian Mangshan Formation; 6—Silurian-Ordovician; 7—Fault; 8—ore body.

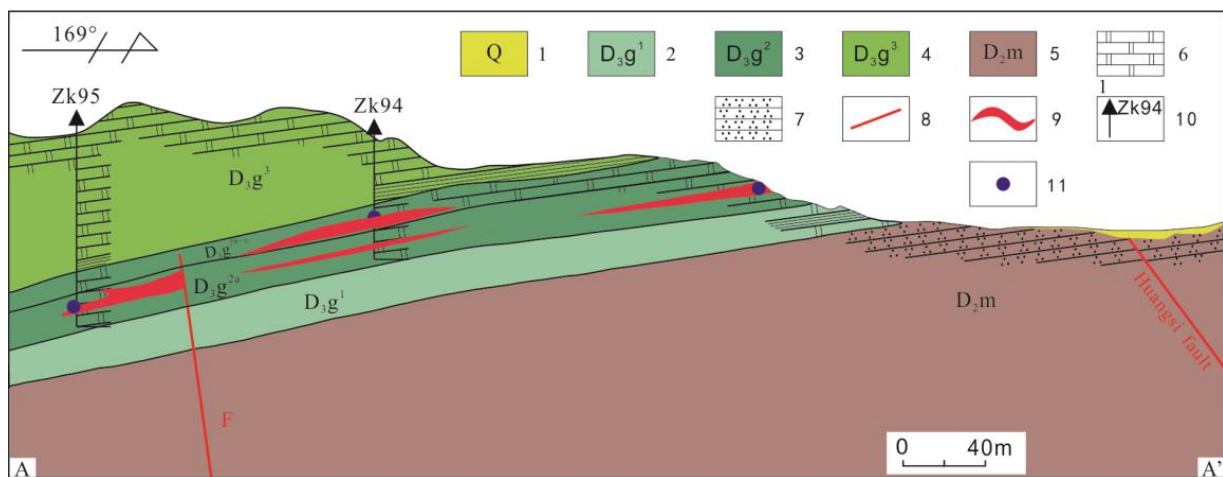


**Figure 3.** The cross-section (A-A') through the Banbianjie Ge-Zn deposit (modified after [13]). 1—Quaternary; 2—first section of the Upper Devonian Gaopochang Formation; 3—second section of the Upper Devonian Gaopochang Formation; 4—third section of the Upper Devonian Gaopochang Formation; 5—Middle Devonian Mangshan Formation; 6—Dolostone; 7—sandstone; 8—fault; 9—ore body; 10—drilling; 11—sample location.

### 3.2. Structure

The mining area is located in the western wing of the wide Huangsi anticline in the regional septal fold assemblage. This assemblage is composed of a series of close synclines and wide anticlines in the near SN-trending and NNE-trending arranged in parallel, and the secondary folds are not developed (Figures 1 and 2). Regional faults are most developed in the near EW trending, and these faults are mostly thickness mutation zones of the Silurian

and Devonian strata and also control the sedimentary evolution of the Carboniferous and Triassic strata, indicating that the faults formed in the late Caledonian. In the subsequent geological process, different degrees of activation occurred, with obvious multi-phase activity characteristics. Among them, the main representative tectonic is the Huangsi fault, which controls sedimentary facies and mineralization [9].

In addition, a new group of the NE-trending structures, with a trend of about  $50^\circ$  and a dip angle of  $75^\circ$ – $80^\circ$ , shows as strike-slip faults (Figure 3). The relationship between the NE-trending structures and mineralization is very obvious. Generally, the closer to this group of structures, the thicker the ore body and the higher the grade. In previous studies, the ore bodies in this deposit are stratiform and veined [38,39]. On the other side of the structures, there are veined ore bodies cutting the bedded ones, which have not been reported before. This is a new understanding of the Banbianjie deposit. The alteration in wall rocks is also developed near the NE-trending structures.

### 3.3. Ore Body

In the Banbianjie Ge-Zn deposit, the Zn metal reserves are more than 0.39 Mt, and the Ge metal resources are more than 900 t [37]. It mainly develops two ore bodies (I and II, Figures 2 and 3); each of them has a total thickness of 3–10 m. The No. I ore body is hosted in  $D_3g^{2b}$  and  $D_3g^{2c}$ , and the ore body floor is the ore-bearing layer floor. The No. II ore body is located in the bottom of  $D_3g^{2a}$ , and the floor is about 15 m away from the sandstone roof of the Mangshan Formation ( $D_2m$ ). The No. II ore body is the main one, and its Zn metal reserve accounts for about 80% of the total Zn metal reserve. The shape of the ore bodies is strata-bound. At the near surface, the occurrence of ore bodies is basically consistent with that of the wall rocks. In the deep part, the irregularly veined ore bodies crosscut the wall rocks (Figure 4). The ore bodies extend over 600 m along the strike, and the ore grades of Zn range from 1.78% to 9.50% (average 5.1%), while the ore grades of Ge range from  $100 \times 10^{-6}$  to  $110 \times 10^{-6}$ . In general, the thicknesses and grades of the ore bodies in this deposit change a little in space.

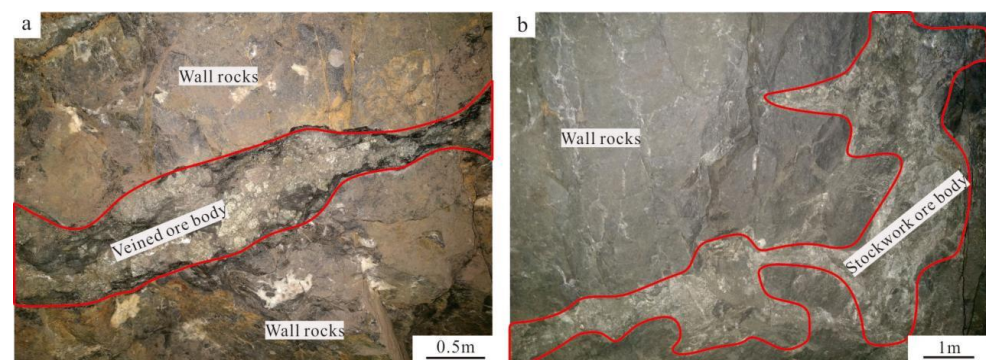


**Figure 4.** Macroscopic characteristics of ore bodies in the Banbianjie Ge-Zn deposit. (a) Veined ore body; (b) stock-work ore body.

### 3.4. Mineralogy

The mineral compositions of the Banbianjie Ge-Zn deposit are relatively simple. Sulfide ore minerals are dominated by sphalerite and pyrite, with minor amounts of marcasite and galena. The gangue minerals are mainly dolomite, calcite and barite, with minor amounts of quartz. There are three main ore types: (i) massive ores, sphalerite coexists with dolomite and calcite (Figure 5a,b); (ii) veined ores, the veins are between 5 cm and 60 cm wide, sphalerite coexists with barite (Figure 5c); and (iii) colloidal ores, sphalerite coexists with dolomite and pyrite (Figure 5d).

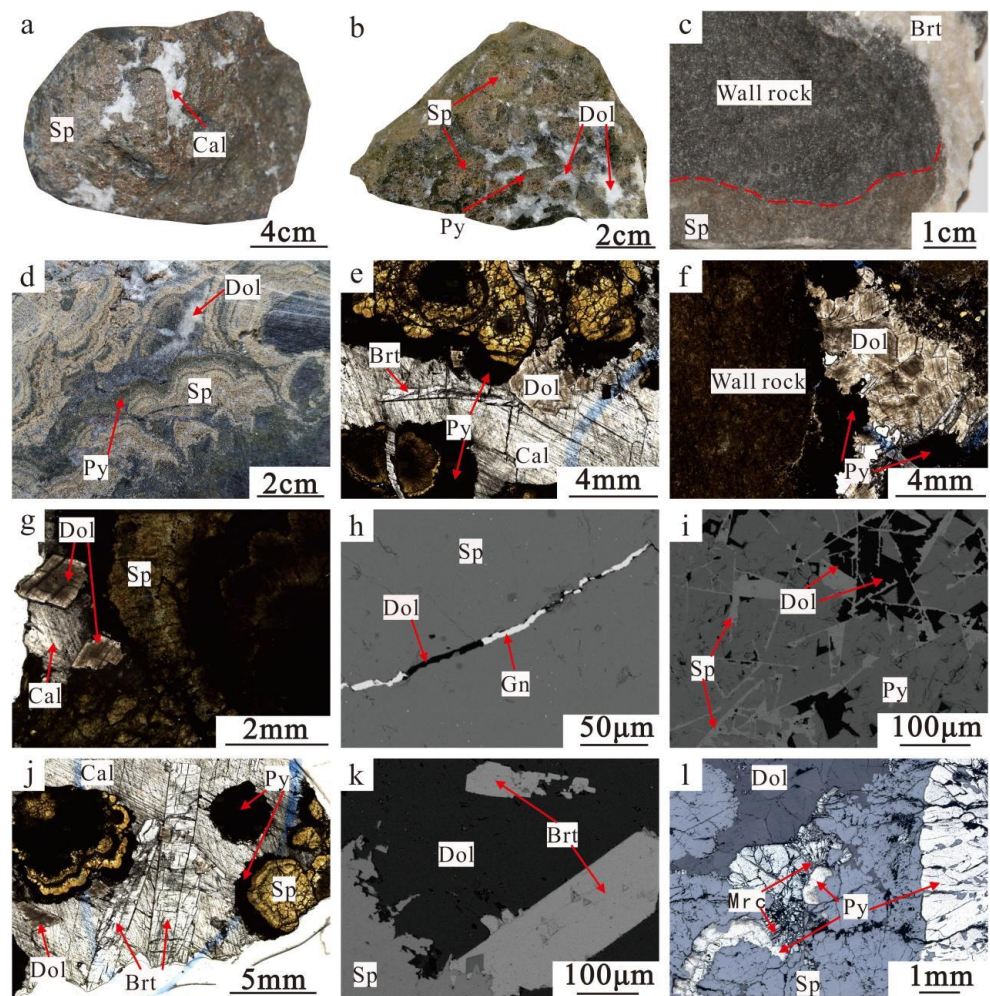


**Figure 5.** Texture and structure characteristics of the Banbianjie Ge-Zn Deposit. (a) Massive ores, sphalerite coexists calcite; (b) massive ores, sphalerite coexists dolomite and pyrite; (c) veined ores, sphalerite coexists barite; (d) colloidal ores, sphalerite coexists with pyrite; (e) dolomite/calcite cement ring-banded sulfides, columnar barite embedded in calcite; (f) granular dolomite cement pyrite in contact with the scarf; (g) granular dolomite is embedded in the sulfides; (h) veined galena and dolomite fill into the fracture of sphalerite; (i) sphalerite replaces pyrite and is cemented by dolomite; (j) sphalerite, pyrite, barite and dolomite are enclosed by calcite; (k) barite is enclosed by dolomite and coexists with sphalerite; (l) marcasite coexists pyrite, sphalerite and dolomite. (Sp = sphalerite; Py = pyrite; Gn = galena; Mrc = marcasite; Dol = dolomite; Cal = calcite; Brt = barite).

Sphalerite has mostly ring ribbon, colloform and metasomatic relict textures (Figure 5d–l), and the veined galena fills into the fracture of sphalerite (Figure 5h). The germanium contents in sphalerite range from  $173 \times 10^{-6}$  to  $1553 \times 10^{-6}$ . Dolomite mainly grows in the outer void of colloidal sphalerite, and the contact of dolomite and sulfides shows fine grain (Figure 5f). Dolomite and calcite exhibit symbiosis (Figure 5g). Hence, dolomite and calcite were formed in the ore-forming stage. Columnar barite is encased in dolomite and grown along the edge of sphalerite (Figure 5j,k), indicating that barite is also a product of the ore-forming stage. The veined calcite fills and cements sulfides. Irregularly, the acicular marcasite coexists with sphalerite or is metasomatized by pyrite. Dolomite with a fine-granular structure (size: 0.5–1.5 mm) is intergrown in the clearance between calcite and sulfides. Columnar barite crosscuts dolomite and calcite (Figure 5k).

### 3.5. Alteration in Wall Rocks

The alteration is relatively simple, and it is dominated by carbonatization and pyritization, with barization and silicification. The pre-ore dolomite is the main mineral formed by carbonatization, which exists near or within the ore body, fault fracture zone and inter-bedded fracture zone and is closely related to Ge-Zn mineralization. It is an important prospecting indicator. Pyritization is closely related to Pb-Zn mineralization and has a wide distribution. Barization formed barite (Figure 5c), and silicification formed quartz and silicified wall rocks.

## 4. Analytical Methods

The whole-rock trace element analysis of barite was undertaken at the State Key Laboratory of Ore Deposit Geochemistry, Institute of Geochemistry, Chinese Academy Sciences (SKLOGD-IGCAS). First, we crushed and screened the fresh samples, washed and dried them with grain sizes between 40 and 60 meshes and selected barite single mineral under the binocular microscope, with a purity greater than 99%. Then, we cleaned them with 75% alcohol and dried at low temperature. Following this, the dried single mineral samples were ground into powder less than 200 meshes in an agate mortar and were acid-dissolved. Finally, the quadrupole-inductively coupled plasma-mass spectrometry (Q-ICPMS) analysis was used to approach the contents. The precisions of REE and other trace elements are better than 5% and 10%, respectively. Please refer to [40] for the detailed analysis process. The repeated analysis results of samples are basically consistent within the error range, and the analysis results of standard samples (OU-6, AGV-2, GBPG-1) are also basically consistent with the recommended values [41–43]. The detection limits are as follows: Tb, Ho, Lu and Tm ( $0.01 \times 10^{-6}$ ); Er, Eu, Sm, Pr and Yb ( $0.03 \times 10^{-6}$ ); Ce, Gd and Dy ( $0.05 \times 10^{-6}$ ); Nd ( $0.1 \times 10^{-6}$ ); Y and La ( $0.5 \times 10^{-6}$ ) [41].

The in situ trace elements analyses of dolomite and calcite were undertaken at the SKLOGD-IGCAS using laser ablation-inductively coupled plasma-mass spectrometry (LA-ICPMS) and employing a standard-sample-standard analysis approach. The instruments used were the ArF excimer laser 193 nm laser system and Agilent 7700X plasma-mass spectrometry, corrected through analysis of SRM610, SRM612 (trace elements in glass), MACS-3 (synthetic calcium carbonate microanalysis reference material), multiple external standard and single internal standard (Ca = 21.7%). The content gap is a huge difference between the Ca and REE, so we used the theoretical values of Ca in the calculation of Yb/Ca ratios. All analyses used 5 Hz laser frequency, 44  $\mu\text{m}$  diameter laser beam, 50 s single measurement time, about 12 s background measurement time and the standard sample was tested once every 15-point analysis. The analysis precision was better than 10%, and the data were processed with ICP-MS DataCal software. For detailed analysis methods, please refer to [44]. The analysis results of standard samples (SRM610, SRM612 and MACS-3) were basically consistent with the recommended values. Three silicate glass reference materials, SRM610, SRM612 and MACS-3, were shown to be homogeneous [45,46]. LA-ICPMS analyses yielded results that agreed with the reference values within relative uncertainties of ca. 5%–10% at a 95% confidence level [45,46].

## 5. Results

The analysis results are shown in Tables 1 and 2, of which the whole-rock REE data of wall rocks (altered dolostone) were taken from [14]. The in situ contents of Mn, Fe and Sr in the dolomite and calcite from the Banbianjie deposit are more than  $69 \times 10^{-6}$ ,  $1 \times 10^{-6}$  and  $22 \times 10^{-6}$ , respectively, and the in situ contents of Pb, Th and U are less than  $8 \times 10^{-6}$ ,  $0.7 \times 10^{-6}$  and  $0.7 \times 10^{-6}$ , respectively. The in situ Ba contents of dolomite and calcite are between  $0.155 \times 10^{-6}$  and  $12.4 \times 10^{-6}$  (Table 1). In barite, the whole-rock contents of Zn and Sr are generally higher than their crustal abundances, while the whole-rock contents of other trace elements are lower than their crustal abundances (Table 2).

**Table 1.** The contents and ratios of in situ trace elements ( $10^{-6}$ ) for dolomite and calcite from the Banbianjie Ge-Zn deposit.

No.	Objection	Mn	Fe	Sr	Ba	Pb	Th	U	Fe/Mn	Sr/Ba	Th/U
BBJ13-2-8	Altered dolostone	123	192	73.0	12.4	0.440	0.330	0.377	1.56	6	0.88
BBJ13-2-9	Altered dolostone	110	253	76.3	9.22	0.996	0.327	0.609	2.30	8	0.54
BBJ13-2-10	Altered dolostone	81.4	227	99.7	5.82	0.375	0.141	0.483	2.79	17	0.29
BBJ9-3-2	Calcite	93.1	14.4	92.5	1.70	0.037	0.096	0.007	0.15	54	14
BBJ9-3-3	Calcite	69.4	17.5	130	0.608	0.114	0.047	0.094	0.25	214	0.50
BBJ9-3-8	Calcite	107	75.6	98.3	0.155	0.058	0.077	0.131	0.71	634	0.59
BBJ9-3-10	Calcite	95.2	-	113	0.644	4.26	0.049	0.011	-	175	4.45
BBJ9-3-11	Calcite	93.8	77.4	131	0.704	0.168	0.073	0.276	0.83	186	0.26
BBJ9-3-1	Dolomite	107	-	28.8	0.583	-	0.118	-	-	49	-
BBJ9-3-4	Dolomite	115	15.3	25.6	0.721	0.005	0.085	-	0.13	36	-
BBJ9-3-5	Dolomite	107	49.8	26.3	0.898	0.744	0.101	0.006	0.47	29	17
BBJ9-3-12	Dolomite	121	-	28.0	1.53	0.070	0.079	-	-	18	-
BBJ9-3-14	Dolomite	121	-	22.7	1.12	0.035	0.118	0.001	-	20	118
BBJ9-3-15	Dolomite	127	-	25.5	-	0.055	0.143	0.002	-	-	72
BBJ2-3-1	Dolomite	134	-	28.5	1.05	0.195	0.098	0.006	-	27	16
BBJ2-3-2	Dolomite	110	6.15	29.1	-	0.015	0.109	0.005	0.06	-	22
BBJ2-3-3	Dolomite	122	1.67	29.8	1.34	0.131	0.100	0.002	0.01	22	50
BBJ2-3-4	Dolomite	109	1.75	36.9	4.54	0.088	0.171	0.003	0.02	8	57
BBJ2-3-5	Dolomite	115	11.5	23.6	1.61	0.024	0.141	-	0.10	15	-
BBJ2-3-6	Dolomite	104	10.0	46.5	-	1.08	0.055	0.004	0.10	-	14
BBJ2-3-7	Dolomite	143	9.44	23.9	1.19	0.051	0.128	0.002	0.07	20	64
BBJ2-3-8	Dolomite	148	35.1	32.8	0.303	0.039	0.124	0.002	0.24	108	62
BBJ2-3-9	Dolomite	146	-	29.3	2.01	0.028	0.187	-	-	15	-
BBJ2-3-10	Dolomite	151	22.8	25.0	1.66	0.016	0.256	0.005	0.15	15	51
BBJ-15-1	Dolomite	86.6	-	118	1.75	1.88	0.335	0.003	-	67	112
BBJ-15-2	Dolomite	95.8	76.4	114	4.60	7.70	0.602	0.024	0.80	25	25
BBJ-15-3	Dolomite	89.2	34.7	103	2.26	0.806	0.329	0.008	0.39	46	41
BBJ-15-4	Dolomite	87.9	11.0	104	3.51	0.150	0.241	0.001	0.13	30	241
BBJ-15-5	Dolomite	140	77.7	35.8	0.235	10.9	0.340	0.013	0.56	152	26
BBJ-15-2-1	Dolomite	119	39.8	78.9	3.74	0.042	0.204	0.007	0.33	21	29
BBJ-15-2-2	Dolomite	159	18.8	37.7	1.62	0.005	0.230	-	0.12	23	-
BBJ-15-2-3	Dolomite	112	-	26.1	0.668	0.048	0.139	-	-	39	-
BBJ-15-2-4	Dolomite	135	22.6	24.4	0.166	0.005	0.187	-	0.17	147	-
BBJ-15-2-5	Dolomite	112	-	24.3	1.37	0.003	0.101	0.003	-	18	34
BBJ-15-2-6	Dolomite	116	-	26.9	1.17	0.019	0.122	-	-	23	-
BBJ-15-2-7	Dolomite	134	29.8	62.3	1.30	0.019	0.136	0.001	0.22	48	136
BBJ-15-2-8	Dolomite	136	90.2	26.2	1.44	2.76	0.254	0.009	0.66	18	28
BBJ-15-2-9	Dolomite	122	11.3	26.6	1.72	0.010	0.104	0.001	0.09	15	104

(Note: “-” indicates that the element contents of the tested sample are lower than those of the detection limitation).

**Table 2.** The whole-rock contents and ratios of trace elements ( $10^{-6}$ ) for barite from the Banbianjie Ge-Zn deposit.

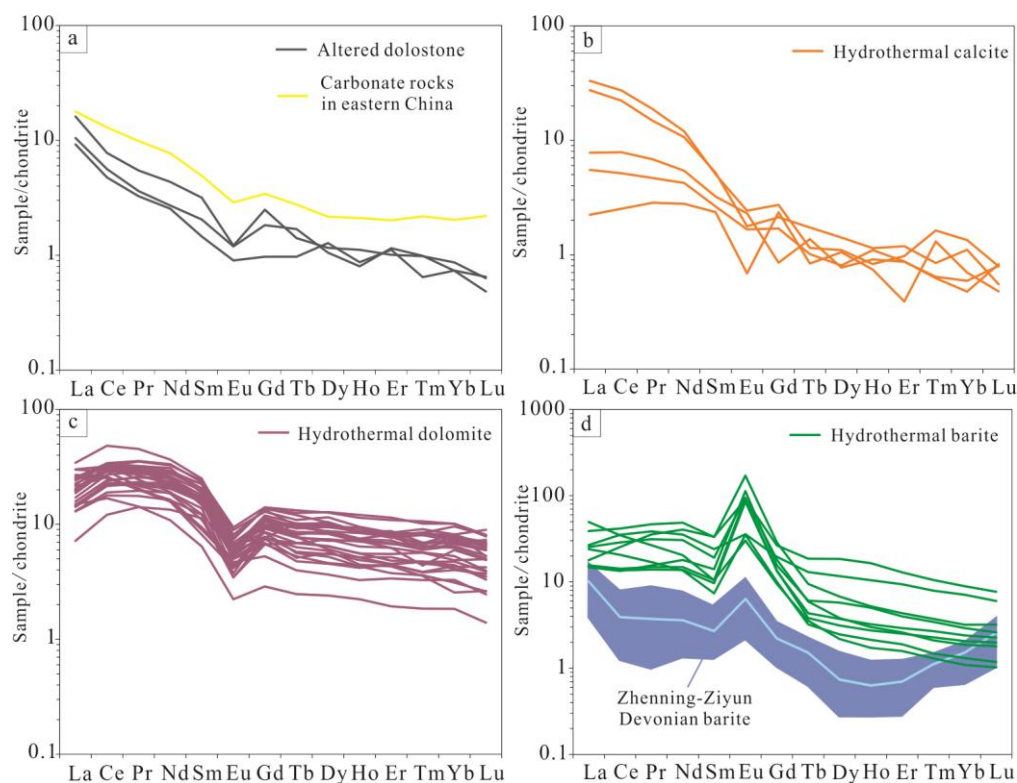
No.	Li	Be	Sc	V	Cr	Co	Ni	Cu	Zn	Ga	Ge	As
BBJ-16	0.613	0.014	0.820	0.451	1.22	6.71	38.8	5.27	869	0.497	1.12	0.632
DY29-1	0.827	0.019	1.53	1.40	0.947	4.07	11.6	8.31	193	0.541	0.495	0.505
BBJ-13	0.693	0.022	0.934	1.10	1.22	5.71	22.1	5.68	66.7	0.546	0.235	0.594
BBJ-14	0.672	0.023	0.906	1.54	1.81	5.87	23.6	5.53	1048	0.397	1.58	0.539
BBJ-1	0.628	0.015	1.07	1.72	1.33	4.82	10.4	7.99	615	0.346	0.714	0.442
BBJ-4	0.554	0.011	1.45	2.13	1.32	3.94	12.4	7.57	348	0.272	0.507	0.445
DY26-3	2.19	0.033	6.51	4.76	2.72	5.85	20.8	14.1	1607	0.901	3.21	1.09
DY2-1	1.01	0.025	1.02	1.82	2.25	4.77	11.9	8.87	115	0.379	0.372	0.690
DY13	0.450	0.015	0.674	1.10	1.11	4.05	18.0	7.28	34.7	0.444	0.177	0.545
Crustal abundances	20	3.0	11	60	35	10	20	25	71	17	1.6	1.5
No.	Ag	Cd	In	Sn	Sb	Cs	Ba	Hf	Ta	W	Tl	Pb
BBJ-16	0.039	1.15	0.005	0.230	0.173	0.010	22426	0.011	0.048	0.215	0.074	110
DY29-1	0.016	0.202	0.009	0.124	0.105	0.020	67975	0.021	0.013	0.110	0.019	3.93
BBJ-13	0.062	0.089	0.006	0.144	0.140	0.015	19052	0.059	0.036	0.197	0.036	8.16
BBJ-14	0.022	1.21	0.007	0.335	0.175	0.009	20889	0.015	0.029	0.191	0.13	28.2
BBJ-1	0.019	0.982	0.006	0.130	0.158	0.009	59948	0.020	0.013	0.117	0.037	4.81

Table 2. Cont.

BBJ-4	0.020	0.412	0.005	0.119	0.245	0.010	54232	0.018	0.011	0.105	0.068	4.95
DY26-3	0.142	3.53	0.040	0.312	0.378	0.016	128938	0.040	0.025	0.149	0.126	29.6
DY2-1	0.049	0.209	0.015	0.154	0.137	0.032	87013	0.044	0.016	0.106	0.015	32.6
DY13	0.021	0.033	0.005	0.107	0.077	0.014	63624	0.091	0.028	0.163	0.002	0.544
Crustal abundances	50	98	50	5.5	0.2	3.7	550	5.8	2.2	2.0	750	20
No.	Rb	Sr	Zr	Nb	Mo	Bi	Th	U	Sr/Ba	Th/U		
BBJ-16	0.153	356	0.105	0.071	0.272	0.009	0.074	0.036	0.02	2		
DY29-1	0.139	774	0.078	0.024	0.150	0.005	0.054	0.008	0.01	7		
BBJ-13	0.138	378	0.094	0.046	0.198	0.004	0.113	0.014	0.02	8		
BBJ-14	0.135	180	0.108	0.040	0.215	0.004	0.107	0.014	0.01	8		
BBJ-1	0.145	1073	0.117	0.018	0.190	0.002	0.104	0.016	0.02	7		
BBJ-4	0.138	896	0.094	0.028	0.187	0.004	0.071	0.011	0.02	6		
DY26-3	0.210	577	0.153	0.042	0.206	0.011	0.155	0.012	0.00	13		
DY2-1	0.217	1047	0.476	0.072	0.203	0.009	0.094	0.025	0.01	4		
DY13	0.115	919	0.111	0.031	0.173	0.005	0.084	0.035	0.01	2		
Crustal abundances	112	350	190	25	1.5	127	10.7	2.8				

(Note: crustal abundances after [1]).

The whole-rock total rare earth element ( $\Sigma\text{REE}$ ) contents of altered dolostone range from  $10.1 \times 10^{-6}$  to  $16.8 \times 10^{-6}$  [14], which are slightly lower than these of hydrothermal calcite, dolomite and barite (Table 3). Altered dolostone is rich in light rare earth elements (LREE) ( $\Sigma\text{LREE}/\Sigma\text{HREE} = 7.4\text{--}9.4$ ,  $\text{La}/\text{Yb}_N = 12.5\text{--}18.6$ ) (Figure 6a) and has negative Eu ( $\text{Eu}/\text{Eu}^* = 0.43\text{--}0.74$ ) and Ce anomalies ( $\text{Ce}/\text{Ce}^* = 0.72\text{--}0.80$ ) [14].



**Figure 6.** Chondrite-normalized REE patterns of whole-rock altered dolostone (a), in situ hydrothermal calcite (b) and dolomite (c), and whole-rock hydrothermal barite (d) from the Banbianjie Ge-Zn deposit (Chondrite values from [47]; whole-rock altered dolostone data are from [14]; carbonate rock data in Eastern China are from [48]; Zhenning–Ziyun Devonian barite data are from [49]).

**Table 3.** REE contents ( $10^{-6}$ ) and statistical parameters of altered dolostone, and hydrothermal calcite, dolomite and barite from the Banbianjie Ge-Zn deposit.

Sample	Altered Dolostone				Hydrothermal Calcite						Hydrothermal Dolomite		
	BBJ13-2-8	BBJ13-2-9	BBJ13-2-10	Average	BBJ9-3-2	BBJ9-3-3	BBJ9-3-8	BBJ9-3-10	BBJ9-3-11	Average	BBJ9-3-1	BBJ9-3-4	BBJ9-3-5
La	2.86	3.25	5.00	3.70	0.692	1.71	10.2	2.41	8.50	4.71	4.46	4.07	4.90
Ce	3.81	4.50	6.21	4.84	2.02	4.12	21.9	6.30	17.8	10.4	17.5	15.2	19.4
Pr	0.398	0.441	0.666	0.502	0.347	0.571	2.29	0.833	1.81	1.17	2.81	2.39	3.13
Nd	1.53	1.63	2.61	1.92	1.67	2.54	7.18	3.25	6.39	4.21	13.7	11.3	15.2
Sm	0.284	0.399	0.619	0.434	0.460	0.515	0.985	0.629	1.01	0.721	3.11	2.69	3.50
Eu	0.066	0.088	0.089	0.081	0.050	0.122	0.178	0.169	0.131	0.130	0.463	0.275	0.467
Gd	0.251	0.474	0.644	0.457	0.609	0.438	0.705	0.221	0.551	0.505	2.60	2.38	2.91
Tb	0.046	0.080	0.067	0.064	0.040	0.048	0.054	0.065	0.082	0.058	0.408	0.363	0.458
Dy	0.410	0.339	0.374	0.374	0.339	0.259	0.353	0.248	0.454	0.331	2.74	2.38	3.38
Ho	0.062	0.058	0.080	0.067	0.053	0.079	0.060	0.065	0.082	0.068	0.535	0.461	0.619
Er	0.234	0.242	0.212	0.229	0.082	0.183	0.204	0.182	0.249	0.180	1.52	1.32	1.67
Tm	0.021	0.032	0.032	0.028	0.042	0.020	0.053	0.021	0.027	0.033	0.195	0.142	0.276
Yb	0.154	0.153	0.181	0.163	0.146	0.099	0.281	0.124	0.231	0.176	1.42	1.25	1.63
Lu	0.021	0.016	0.020	0.019	0.015	0.027	0.026	0.026	0.018	0.022	0.192	0.158	0.227
Y	2.54	2.92	3.16	2.87	1.30	2.08	1.77	1.97	2.56	1.94	14.4	12.4	17.4
ΣREE	10.1	11.7	16.8	12.9	6.56	10.7	44.5	14.6	37.3	22.7	51.7	44.4	57.8
LREE	8.94	10.3	15.2	11.5	5.24	9.58	42.7	13.6	35.6	21.4	42.1	36.0	46.6
HREE	1.20	1.39	1.61	1.40	1.33	1.15	1.73	0.95	1.70	1.37	9.62	8.45	11.2
LREE/HREE	7.45	7.40	9.44	8.10	3.95	8.30	24.63	14.28	21.02	14.43	4.38	4.25	4.17
La/Yb <sub>N</sub>	12.54	14.33	18.61	15.16	3.20	11.57	24.60	13.15	24.76	15.46	2.12	2.19	2.02
La/Sm <sub>N</sub>	6.34	5.12	5.08	5.51	0.95	2.08	6.55	2.41	5.27	3.45	0.90	0.95	0.88
Eu/Eu*	0.74	0.61	0.43	0.59	0.29	0.77	0.62	1.13	0.48	0.66	0.48	0.33	0.44
δCe	0.76	0.80	0.72	0.76	0.99	1.01	1.06	1.08	1.05	1.04	1.17	1.16	1.17

Sample	Hydrothermal dolomite												
	BBJ9-3-12	BBJ9-3-14	BBJ9-3-15	BBJ2-3-1	BBJ2-3-2	BBJ2-3-3	BBJ2-3-4	BBJ2-3-5	BBJ2-3-6	BBJ2-3-7	BBJ2-3-8	BBJ2-3-9	BBJ2-3-10
La	4.02	6.38	6.87	4.52	4.40	4.59	5.31	6.14	2.23	5.81	4.51	7.06	7.93
Ce	14.3	24.5	27.3	17.7	17.3	17.9	21.7	23.0	9.70	23.6	18.1	24.0	27.2
Pr	2.16	3.87	4.34	2.68	2.78	2.67	3.49	3.59	1.73	3.69	2.85	3.29	3.74
Nd	9.76	17.4	20.1	13.1	12.6	12.3	16.5	15.7	8.08	16.8	13.4	13.3	15.6
Sm	2.36	4.02	4.56	3.04	3.08	3.06	4.41	3.82	2.20	4.00	3.36	3.10	2.86
Eu	0.254	0.475	0.562	0.480	0.307	0.371	0.656	0.431	0.255	0.507	0.411	0.387	0.495
Gd	1.93	2.41	3.56	2.55	2.43	1.98	3.34	2.97	1.74	2.82	2.90	2.21	2.00
Tb	0.326	0.482	0.570	0.385	0.367	0.481	0.518	0.448	0.324	0.457	0.456	0.267	0.300

Table 3. Cont.

Dy	2.09	3.12	3.35	2.82	2.32	3.30	3.71	2.80	2.39	3.10	3.05	1.69	1.90
Ho	0.400	0.669	0.611	0.541	0.525	0.620	0.685	0.604	0.509	0.631	0.628	0.310	0.321
Er	1.16	1.70	1.66	1.71	1.44	1.84	1.78	1.64	1.44	1.77	1.61	0.791	0.906
Tm	0.183	0.273	0.272	0.216	0.222	0.225	0.295	0.203	0.195	0.261	0.262	0.117	0.115
Yb	1.02	2.00	1.59	1.59	1.72	1.43	1.71	1.51	1.35	1.52	1.61	0.651	0.535
Lu	0.161	0.260	0.222	0.204	0.170	0.237	0.289	0.220	0.172	0.211	0.217	0.084	0.085
Y	11.4	17.9	17.8	14.5	13.4	16.4	19.2	16.6	13.3	16.8	18.2	10.2	11.0
ΣREE	40.2	67.6	75.5	51.5	49.6	51.0	64.4	63.1	32.3	65.2	53.4	57.3	64.0
LREE	32.9	56.7	63.7	41.5	40.4	40.9	52.1	52.7	24.2	54.4	42.7	51.2	57.9
HREE	7.28	10.9	11.8	10.0	9.19	10.1	12.3	10.4	8.12	10.8	10.7	6.11	6.16
LREE/HREE	4.52	5.20	5.39	4.14	4.39	4.04	4.22	5.07	2.98	5.06	3.98	8.37	9.39
La/Yb <sub>N</sub>	2.66	2.15	2.92	1.91	1.73	2.16	2.09	2.73	1.11	2.58	1.89	7.31	10.0
La/Sm <sub>N</sub>	1.07	1.00	0.95	0.94	0.90	0.94	0.76	1.01	0.64	0.91	0.84	1.43	1.74
Eu/Eu*	0.35	0.43	0.41	0.51	0.33	0.43	0.50	0.38	0.39	0.44	0.39	0.43	0.60
δCe	1.17	1.17	1.18	1.21	1.17	1.22	1.18	1.17	1.14	1.20	1.20	1.21	1.21
<b>Hydrothermal dolomite</b>													
<b>Sample</b>	<b>BBJ15-1</b>	<b>BBJ15-2</b>	<b>BBJ15-3</b>	<b>BBJ15-4</b>	<b>BBJ15-5</b>	<b>BBJ15-2-1</b>	<b>BBJ15-2-2</b>	<b>BBJ15-2-3</b>	<b>BBJ15-2-4</b>	<b>BBJ15-2-5</b>	<b>BBJ15-2-6</b>	<b>BBJ15-2-7</b>	<b>BBJ15-2-8</b>
La	9.29	8.36	7.87	9.35	8.02	6.70	7.51	7.62	5.99	6.11	4.91	4.64	10.7
Ce	23.2	20.8	20.3	25.6	26.0	20.6	25.8	27.0	23.8	24.6	19.0	13.5	38.7
Pr	2.63	2.43	2.44	3.00	3.71	2.51	3.56	3.93	3.41	3.91	3.17	1.75	5.54
Nd	11.1	9.84	9.46	11.5	15.7	9.52	15.0	18.6	14.9	17.5	14.2	6.52	22.0
Sm	2.14	1.85	1.59	2.40	3.20	1.76	3.13	3.66	2.89	4.36	3.05	1.25	4.89
Eu	0.326	0.366	0.306	0.424	0.467	0.345	0.455	0.462	0.441	0.543	0.392	0.164	0.600
Gd	1.94	1.74	1.78	2.03	2.23	1.37	2.48	3.10	2.76	3.57	2.76	0.748	3.47
Tb	0.243	0.250	0.226	0.273	0.328	0.189	0.368	0.483	0.397	0.597	0.438	0.117	0.463
Dy	1.81	1.48	1.47	1.78	2.07	1.18	1.96	3.17	2.66	4.13	3.05	0.774	2.78
Ho	0.350	0.315	0.300	0.372	0.403	0.235	0.369	0.608	0.512	0.868	0.638	0.160	0.515
Er	0.953	0.936	0.939	1.09	1.02	0.712	0.95	1.63	1.42	2.41	1.80	0.407	1.31
Tm	0.153	0.124	0.125	0.148	0.154	0.106	0.153	0.224	0.210	0.329	0.266	0.060	0.185
Yb	0.992	0.836	0.908	0.898	0.858	0.688	0.929	1.47	1.31	2.12	1.70	0.386	1.11
Lu	0.125	0.120	0.113	0.136	0.114	0.080	0.107	0.197	0.162	0.262	0.215	0.045	0.127
Y	10.0	8.93	8.66	9.94	12.3	6.37	12.1	15.7	13.8	21.8	16.2	3.98	15.3
ΣREE	55.2	49.5	47.9	59.0	64.2	46.0	62.7	72.1	60.9	71.4	55.6	30.5	92.3
LREE	48.7	43.7	42.0	52.3	57.0	41.4	55.4	61.2	51.5	57.1	44.7	27.8	82.4
HREE	6.57	5.80	5.86	6.73	7.17	4.56	7.31	10.9	9.42	14.3	10.9	2.70	9.95
LREE/HREE	7.41	7.53	7.17	7.77	7.95	9.09	7.58	5.62	5.46	4.00	4.11	10.32	8.28

Table 3. Cont.

La/Yb <sub>N</sub>	6.31	6.74	5.84	7.02	6.30	6.56	5.45	3.48	3.09	1.94	1.94	8.10	6.51
La/Sm <sub>N</sub>	2.73	2.85	3.11	2.45	1.57	2.40	1.51	1.31	1.31	0.88	1.01	2.32	1.37
Eu/Eu*	0.48	0.62	0.55	0.57	0.51	0.66	0.48	0.41	0.47	0.41	0.41	0.48	0.42
δCe	1.12	1.11	1.12	1.17	1.16	1.22	1.21	1.19	1.26	1.19	1.14	1.15	1.21
Sample	Hydrothermal dolomite			Hydrothermal barite									
	BBJ-15-2-9	Average		BBJ-16	DY29-1	BBJ-13	BBJ-14	BBJ-1	BBJ-4	DY26-3	DY2-1	DY13	Average
La	6.28	6.22		15.4	7.9	8.33	7.47	4.7	4.85	12.1	4.59	5.57	7.88
Ce	25.8	21.8		27.9	23	28.3	16.5	10.9	11.4	33.3	10.7	20.4	20.3
Pr	4.31	3.18		3.25	3.83	4.72	2.08	1.7	1.82	5.69	1.9	4.35	3.26
Nd	19.6	14.01		12.3	18.4	21.3	8.19	8.27	8.92	29.3	10.8	24.3	15.8
Sm	4.7	3.13		2.05	3.74	4.69	1.44	1.89	2.06	6.47	2.74	6.55	3.51
Eu	0.692	0.426		2.22	7	2.63	2.59	6.28	6.78	12.6	8.35	6.65	6.12
Gd	3.65	2.48		2.46	4.7	5.07	2.6	3.53	3.46	7.47	4.06	6.88	4.47
Tb	0.628	0.387		0.169	0.281	0.618	0.153	0.181	0.206	0.451	0.289	0.884	0.359
Dy	4.07	2.55		0.705	1.23	3.76	0.794	1.01	1.2	2.19	1.86	5.96	2.08
Ho	0.82	0.504		0.124	0.215	0.752	0.153	0.197	0.233	0.375	0.362	1.19	0.4
Er	2.29	1.39		0.333	0.546	1.98	0.397	0.53	0.612	0.914	0.836	2.71	0.984
Tm	0.344	0.201		0.042	0.068	0.257	0.048	0.074	0.087	0.121	0.112	0.341	0.128
Yb	2.12	1.3		0.228	0.39	1.49	0.274	0.431	0.503	0.667	0.61	1.87	0.718
Lu	0.253	0.172		0.033	0.058	0.194	0.038	0.064	0.073	0.103	0.084	0.248	0.099
Y	21.4	13.9		5.12	8.94	22	5.86	7.51	8.01	15	13.3	35.1	13.4
ΣREE	75.5	57.7		67.2	71.4	84.1	42.7	39.8	42.2	112	47.3	87.9	66
LREE	61.3	48.7		63.1	63.9	70	38.3	33.7	35.8	99.4	39.1	67.8	56.8
HREE	14.2	8.98		4.09	7.49	14.1	4.46	6.02	6.37	12.3	8.21	20.1	9.24
LREE/HREE	4.33	5.87		15.4	8.53	4.96	8.59	5.61	5.62	8.09	4.76	3.38	7.22
(La/Yb) <sub>N</sub>	2	3.96		45.5	13.7	3.77	18.38	7.35	6.5	12.2	5.07	2.01	12.7
(La/Sm) <sub>N</sub>	0.84	1.38		4.73	1.33	1.12	3.26	1.56	1.48	1.17	1.05	0.54	1.8
Eu/Eu*	0.49	0.46		3.02	5.1	1.64	4.04	7.33	7.71	5.53	7.65	3.01	5
δCe	1.16	1.18		0.91	1.01	1.08	1	0.94	0.93	0.97	0.88	0.95	0.96

(Note: data of BBJ13-2-8, -9 and -10 are from [14], Standardized REE data for chondrites are from [46];  $\delta\text{Ce} = \text{Ce}_N / (\text{La}_N \times \text{Pr}_N)^{1/2}$ ,  $\text{Eu}/\text{Eu}^* = \text{Eu}_N / (\text{Sm}_N \times \text{Gd}_N)^{1/2}$ ).

Hydrothermal calcite and dolomite are also rich in LREE ( $\Sigma\text{LREE}/\Sigma\text{HREE} = 4.0\text{--}24.6$ ,  $\text{La}/\text{Yb}_N = 3.20\text{--}24.78$  and  $\Sigma\text{LREE}/\Sigma\text{HREE} = 2.98\text{--}10.3$ ,  $\text{La}/\text{Yb}_N = 1.11\text{--}10.0$ , respectively), with changed Eu and Ce anomalies ( $\text{Eu}/\text{Eu}^* = 0.29\text{--}1.13$  and  $\text{Ce}/\text{Ce}^* = 0.99\text{--}1.08$ ) (Figure 6b,c) and negative Eu ( $\text{Eu}/\text{Eu}^* = 0.33\text{--}0.66$ ) and positive Ce anomalies ( $\text{Ce}/\text{Ce}^* = 1.11\text{--}1.26$ ), respectively. Hydrothermal barite also has the characteristics of LREE enrichment ( $\Sigma\text{LREE}/\Sigma\text{HREE} = 3.38\text{--}15.42$ ,  $\text{La}/\text{Yb}_N = 2.01\text{--}45.5$ ) (Figure 6d) but with significantly positive Eu ( $\text{Eu}/\text{Eu}^* = 1.64\text{--}7.71$ ) and insignificant Ce anomalies ( $\text{Ce}/\text{Ce}^* = 0.88\text{--}1.08$ ) (Table 3).

## 6. Discussion

### 6.1. The Nature and Source of Ore-Forming Fluids

Previous studies have suggested that the trace element characteristics of hydrothermal gangue minerals (i.e., calcite, dolomite and barite) can indicate the nature and source of ore-forming fluids [50–52]. The evidence of mineralogy (Figure 5) suggests that these gangue minerals formed in the ore-forming stage, so they are hydrothermal minerals. Their trace elements suggest that Sr, Ba, Zn, Fe, Pb and Ge are enriched in the hydrothermal fluids. This is also confirmed by the form of mineral assemblage, such as Sr-rich barite, Ge-rich sphalerite, pyrite and galena (Figure 5). In addition, barite contains variable contents of other trace elements but generally has a similar variation trend, such as systematic enrichment of large ionic lithophile elements and depletion of high-field-strength elements (Figure 7). This is consistent with the basin brine characteristics of MVT deposits (Tables 2 and 3 [53]). Furthermore, the high-temperature metallogenic elements (such as Co, Ni, Mo and Bi) show obviously depleted characteristics (Figure 7), indicating that these deposits have nothing to do with high-temperature magmatism. Therefore, the nature of ore-forming fluids is low-temperature basin brine.

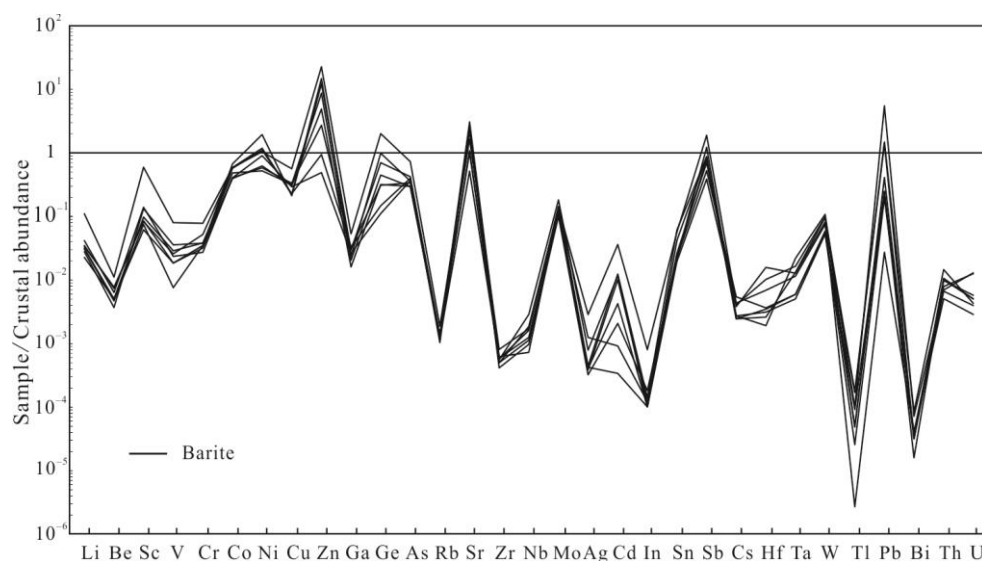


**Figure 7.** The enrichment degree of trace elements in barite relative to crustal abundances for the Banbianjie deposit (crustal abundances after [1]).

Rare earth elements (REEs) record important information about hydrothermal fluids [54–61]. For example, the Tb/Ca-Tb/La diagram (Figure 8) can effectively determine the genesis of calcite [62]. The calcite from the Banbianjie deposit was plotted into the hydrothermal genesis zone (since the difference in the contents between Ca and REE is more than 5 orders of magnitude, the author directly uses the theoretical values of Ca when calculating the Yb/Ca ratios) in the plot of Tb/Ca-Tb/La (Figure 8), indicating hydrothermal genesis, which is consistent with the actual geology. It is obvious that calcite coexists with sulfide minerals in mineral assemblages (Figure 5). Hence, the Banbianjie deposit may not be genetically related to magmatism or sedimentation.

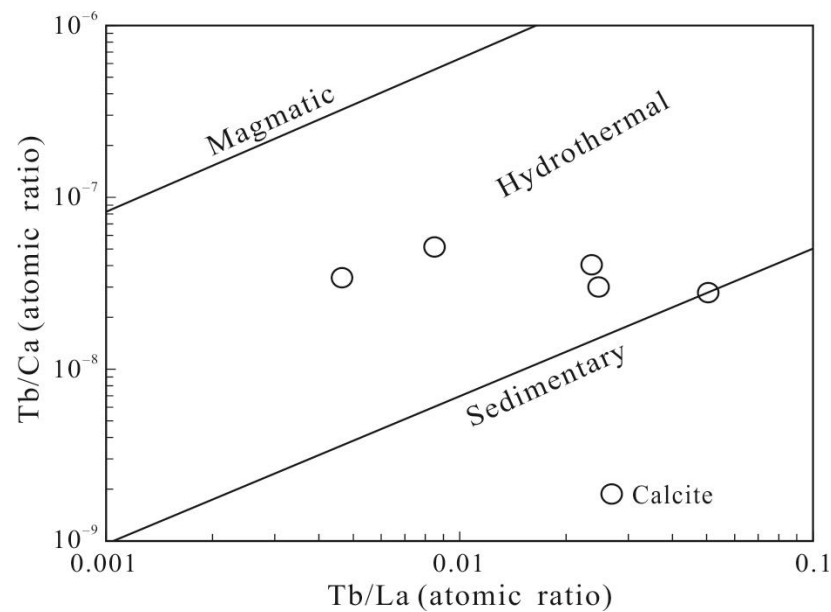


**Figure 8.** Tb/Ca-Tb/La diagram of calcites from Banbianjie Ge-Zn deposit (after [62]).

The La/Ho-Y/Ho diagram (Figure 9a) can identify the cognate of minerals [63]. The hydrothermal dolomite, calcite and barite from the Banbianjie deposit are distributed horizontally in the diagram of La/Ho-Y/Ho (Figure 9a), suggesting that they are the evolution products of the same fluids. This is also supported by the mineral assemblages, dolomite and calcite, which coexist with barite (Figure 5).

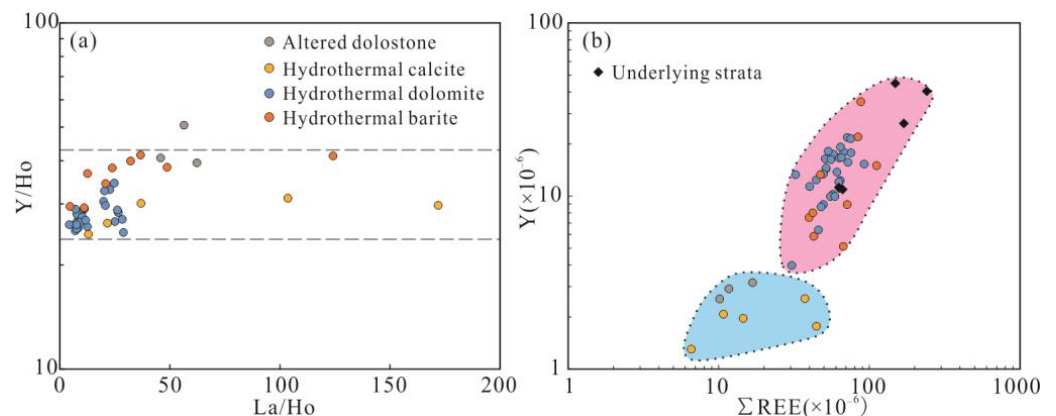


**Figure 9.** La/Ho vs. Y/Ho (a) and Y vs.  $\Sigma$ REE (b), the underlying strata data are from [64] diagrams of the Banbianjie Ge-Zn deposit.

On the chondrite-standardized distribution diagram of REE (Figure 6), dolomite, calcite and barite have the characteristics of LREE enrichment, which further suggests that there is an intrinsic genesis relationship between them, although the ore-forming fluids were not directly or wholly contributed by the wall rocks.

In the Banbianjie deposit, the  $\Sigma$ REE contents of hydrothermal dolomite and barite are significantly higher than those of altered dolostone and hydrothermal calcite (Table 3). As the  $\Sigma$ REE contents of quartz and sulfide minerals are negligible [12,63–65], so the  $\Sigma$ REE contents of hydrothermal dolomite and barite can approximately represent the  $\Sigma$ REE contents of the fluids ( $\Sigma$ REE<sub>dolomite+barite</sub>  $\approx$   $\Sigma$ REE<sub>fluids</sub>). In Figure 6, the  $\Sigma$ REE contents of dolomite and barite are significantly higher than those of both altered dolostone and carbonate rocks in Eastern China. Therefore, the REEs in the ore-forming fluids cannot be completely contributed by ore-bearing carbonate rocks [56], but it cannot be ruled out that

some REEs are inherited from wall rocks during the water/rock (W/R) interaction between ore-forming fluids and wall rocks.

Y and REEs are close in radius, and both are considered to have similar geochemical natures. Therefore, using the variation trend between Y and REE is one of the effective methods to determine the source of fluids [63–65]. In the diagram of Y- $\Sigma$ REE (Figure 9b), the hydrothermal dolomite, calcite and barite are mainly distributed in two concentrated zones. The hydrothermal dolomite and barite that represent the  $\Sigma$ REE contents of the ore-forming fluids are located between altered dolostone and the underlying strata [64]. This indicates that REEs in the ore-forming fluids were likely to be provided by the wall rocks and underlying strata. The results are consistent with the study on the chemical characteristics of carbonate minerals in the adjacent Zhulingou deposit [6]. In summary, the ore-forming fluids of the Banbianjie deposit that are similar to the basin brine may originate from and/or flow through the underlying strata, and parts of ore-forming materials in the fluids are inherited from wall rocks during the water/rock (W/R) interaction.

### 6.2. Evolution of Ore-Forming Fluids

The trace elements of altered dolostone and hydrothermal dolomite and calcite show that they have different ratios of Fe/Mn, Sr/Ba and Th/U (Table 1). For example, the Fe/Mn ratios (1.56–2.79) of altered dolostone are higher than those of hydrothermal calcite and dolomite (0.01–0.83). This suggests that the initial ore-forming fluids have high Fe/Mn ratios. In contrast, the Sr/Ba ratios of hydrothermal calcite and dolomite (8–634) are higher than those of altered dolostone (6–17). This indicates that the Sr/Ba ratios are increased during the mineralization process. In addition, the Th/U ratios of altered dolostone from the Banbianjie deposit are between 0.29 and 0.88, which are quite different from those of hydrothermal calcite and dolomite (0.26–241) and barite (2–13). This implies that the Th/U ratios of hydrothermal fluids have an evolutionary trend of increasing first and then decreasing.

The REE<sup>3+</sup> ion has different geochemical characteristics from those of the Eu<sup>2+</sup> and Ce<sup>4+</sup> ions [66–69]. Therefore, the Eu<sup>2+</sup> and Ce<sup>4+</sup> ions are separated from REE<sup>3+</sup> in the change process of fluid physical and chemical environments, resulting in positive or negative Eu and Ce anomalies, which is called the oxidation reduction mode of REEs [69,70]. Hence, europium (Eu) and cerium (Ce) anomalies are often used to discuss the change in physical–chemical condition during the evolution of hydrothermal fluids [68–78].

There are obviously negative Eu and Ce anomalies in altered dolostone (Figure 6a) and obviously negative Eu and positive Ce anomalies of hydrothermal calcite and dolomite (Figure 6c), as the ore-forming fluids originated from and/or flowed through the underlying strata and interacted with wall rocks. Hence, the ore-forming fluids were acidic reduced during the early mineralization stage, which is consistent with the fluids' characteristics reflected in the presence of the acicular marcasite ( $T < 240$  °C,  $pH < 5$ , Figure 5l, [38]). Moreover, barite has significant positive Eu anomalies (Figure 6d), and the late stage of the Banbianjie deposit is an open environment, suggesting that the late ore-forming fluids were oxidized. Therefore, the evolution of ore-forming fluids experienced a shift from reduction to oxidation during the Ge-Zn mineralization.

### 6.3. Ore Genesis

There are great controversies on the ore genesis of the Banbianjie Ge-Zn deposit, including: (i) sedimentary exhalative (SEDEX) deposit [9]; (ii) syn-sedimentary modified stratigraphically controlled deposit [38]; and (iii) the Mississippi Valley-type (MVT) deposit [13,14].

According to the geological survey, the Banbianjie Ge-Zn deposit has veined and stock-work ores with metasomatism (Figure 5) and developed the veined ore body that crosscuts the wall rocks (Figure 4b). These structures and textures of ores and hydrothermal minerals suggest the characteristics of epigenetic mineralization. In addition, more than 200 Pb-Zn deposits have been found in the Western Hunan–Eastern Guizhou Pb-Zn metallogenic belt,

which are mainly hosted by carbonate rocks of the Cambrian to Devonian, and their ore-forming ages are 349–477 Ma (concentrated in 410–450 Ma) [6,10,31]. Hence, this deposit cannot be a SEDEX deposit. The genesis of hydrothermal calcite also excludes the genetic connection between the deposit and magmatism or sedimentation (Figure 8).

The REE patterns and La/Yb<sub>N</sub> ratios of barite can be used to distinguish the ore genesis [48]. The La/Yb<sub>N</sub> values of barite from the Banbianjie deposit are similar to those of the Lehong MVT Pb-Zn deposit in Yunnan province, suggesting that their ore genesis is similar, and both belong to MVT deposits [25]. In addition, barite of the Banbianjie deposit has significantly different REE characteristics from those of the Zhenning–Ziyun Devonian large-scale hot-water sedimentary barite deposits (Figure 6d, [48]), the Guangxi hot-water sedimentary barite deposits [79] and magmatic genesis barite deposits [80]. This shows that the Banbianjie deposit has nothing to do with hot-water precipitation and high-temperature magmatism.

The geological characteristics of most Pb-Zn deposits in the Western Hunan–Eastern Guizhou Pb-Zn metallogenic belt are very similar to those of MVT deposits: (i) all deposits occurred in carbonate sequences; (ii) all deposits are controlled by structures; (iii) with obvious epigenetic metallogenic characteristics; (iv) Pb-Zn mineralization has no relationship with magmatism in time and space; (v) the ore bodies occur mainly as strata bound; and (vi) the ore-forming fluids are medium–low temperatures (120–220 °C) and medium–high salinities (8–23 wt.% NaCl equiv.) [4,12–14,18,81,82]. Hence, they can be classified as MVT deposits.

## 7. Conclusions

1. The trace elements of hydrothermal minerals indicate that the ore-forming fluids are rich in Sr, Ba, Zn, Fe, Pb and Ge, which are similar to those of basin brine. The REE characteristics of hydrothermal minerals suggest that the ore-forming fluids of the Banbianjie deposit were likely derived from and/or flowed through the underlying strata and interacted with wall rocks.
2. The Eu and Ce anomalies of the gangue minerals from the Banbianjie deposit and the mineral assemblages imply that the evolution of ore-forming fluids experienced a shift from reduction to oxidation during Ge-Zn mineralization.
3. The ore deposit geology, mineralogy and trace element geochemistry of the gangue minerals imply that the ore genesis of the Banbianjie deposit is best classified as an MVT deposit.

**Author Contributions:** Investigation, formal analysis, writing—original draft, Y.-L.A.; methodology, supervision, writing—review and editing, J.-X.Z.; writing—review and editing, Q.-T.M., G.-T.S. and Z.-M.Y. All authors have read and agreed to the published version of the manuscript.

**Funding:** This research was funded by the National Natural Science Foundation of China [grant numbers U1812402 and 42172082], Yunnan University Scientific Research Start-up Project [grant number YJRC4201804] and the Major collaborative innovation projects for prospecting breakthrough strategic action of Guizhou Province, China ((2022) ZD004).

**Data Availability Statement:** The data presented in this study are available on reasonable request from the corresponding authors.

**Acknowledgments:** The field work was supported and assisted by workers of the Nos. 104 and 109 Geological Teams of Guizhou Bureau of Geology and Mineral Exploration & Development. The experimental process was guided and assisted by the staff of the State Key Laboratory of Ore Deposit Geochemistry, Institute of Geochemistry, Chinese Academy of Sciences. We would like to express our heartfelt thanks to them!

**Conflicts of Interest:** The authors declare no conflict of interest.

## References

1. Taylor, S.R.; McLennan, S.M. The geochemical evolution of the continental crust. *Rev. Geophys.* **1995**, *33*, 241–265. [[CrossRef](#)]
2. Tu, G.Z.; Gao, Z.M.; Hu, R.Z.; Li, C.Y.; Zhao, Z.H.; Zhang, B.G. *Geochemistry and Metallogenic Mechanism of Disperse Elements*; Geology Press: Beijing, China, 2004. (In Chinese)
3. Wen, H.J.; Zhu, C.W.; Du, S.J.; Fan, Y.; Luo, C.G. Gallium (Ga), germanium (Ge), thallium (Tl) and cadmium (Cd) resources in China. *Sci. Bull.* **2020**, *65*, 3688–3699. (In Chinese with English Abstract) [[CrossRef](#)]
4. Ye, L.; Cook, N.J.; Liu, T.G.; Ciobanu, C.L.; Gao, W.; Yang, Y.L. The Niujaotang Cd-rich zinc deposit, Duyun, Guizhou province, southwest China: Ore genesis and mechanisms of cadmium concentration. *Miner. Deposita* **2012**, *47*, 683–700. [[CrossRef](#)]
5. Luo, K.; Cugerone, A.; Zhou, M.F.; Zhou, J.X.; Sun, G.T.; Xu, J.; He, K.J.; Lu, M.D. Germanium enrichment in sphalerite with acicular and euhedral textures: An example from the Zhulingou carbonate-hosted Zn(-Ge) deposit, South China. *Miner. Deposita* **2022**, *57*, 1343–1365. [[CrossRef](#)]
6. Yang, Z.M.; Zhou, J.X.; Lou, K.; Yang, D.Z.; Yu, J.; Zhou, F.C. Mineralogy and mineral chemistry of carbonates from the Zhulingou Ge-Zn deposit in Guizhou Province and its geological significance. *Acta Petrol. Sin.* **2021**, *37*, 2743–2760. (In Chinese with English Abstract)
7. Zhou, J.X.; Yang, Z.M.; An, Y.L.; Luo, K.; Liu, C.X.; Ju, Y.W. An evolving MVT hydrothermal system: Insights from the Niujaotang Cd-Zn ore field, SW China. *J. Asian Earth Sci.* **2022**, *237*, 105357. [[CrossRef](#)]
8. Wen, H.J.; Zhou, Z.B.; Zhu, C.W.; Luo, C.G.; Wang, D.Z.; Du, S.J.; Li, X.F.; Chen, M.H.; Li, H.Y. Critical scientific issues of super-enrichment of dispersed metals. *Acta. Petrol. Sin.* **2019**, *35*, 327–3291. (In Chinese with English Abstract)
9. Chen, G.Y.; An, Q.; Wang, M. Geological Characteristics and Genesis of the Banbianjie Type Lead-Zinc Deposits in Southern Guizhou Province. *Acta Geosci. Sin.* **2006**, *27*, 570–576. (In Chinese with English Abstract)
10. Ye, L.; Pang, Z.P.; Li, C.Y.; Liu, T.G.; Xia, B. Isotopic Geochemical Characters in Niujaotang Cd Rich Zinc Deposit, Duyun, Guizhou. *J. Mineral. Petrol.* **2005**, *25*, 70–74. (In Chinese with English Abstract)
11. Zhou, J.X.; Huang, Z.L.; Zhou, M.F.; Li, X.B.; Jin, Z.G. Constraints of C-O-S-Pb isotope compositions and Rb-Sr isotopic age on the origin of the Tianqiao carbonate-hosted Pb-Zn deposit, SW China. *Ore Geol. Rev.* **2013**, *53*, 77–92. [[CrossRef](#)]
12. Li, K.; Tang, C.Y.; Liu, J.S.; Cai, Y.X.; Liu, F. Sources of metallogenic materials of Xiunao Pb-Zn deposit in eastern Guizhou: Constraints from REE and C, O, S, Pb isotope geochemistry. *J. Guilin Univ. Technol.* **2018**, *38*, 365–376. (In Chinese with English Abstract)
13. Meng, Q.T.; Zhou, J.X.; Sun, G.T.; Zhao, Z.; An, Q.; Yang, X.Y.; Lu, M.D.; Xiao, K.; Xu, L. Geochemical characteristics and ore prospecting progress of the Banbianjie Zn deposit in Guiding City, Guizhou Province, China. *Acta Mineral. Sin.* **2022**, *42*, 51–58. (In Chinese with English Abstract)
14. An, Y.L.; Luo, K.; Zhou, J.X.; Nguyen, A.; Lu, M.D.; Meng, Q.T.; An, Q. Origin of the Devonian carbonate-hosted Banbianjie Ge-Zn deposit, Guizhou Province, South China: Geological, mineralogical and geochemical constraints. *Ore Geol. Rev.* **2022**, *142*, 104696. [[CrossRef](#)]
15. Zhou, J.X.; Huang, Z.L.; Zhou, G.F.; Jin, Z.G.; Li, X.B.; Ding, W.; Gu, J. Sources of the Ore Metals of the Tianqiao Pb-Zn Deposit in Northwestern Guizhou Province: Constraints form S, Pb Isotope and REE Geochemistry. *Geol. Rev.* **2010**, *56*, 513–524. (In Chinese with English Abstract)
16. Zhou, J.X.; Huang, Z.L.; Zhou, G.F.; Zeng, Q.S. C, O Isotope and REE Geochemistry of the Hydrothermal Calcites from the Tianqiao Pb-Zn Ore Deposit in NW Guizhou Province, China. *Geotecton. Metallog.* **2012**, *36*, 93–101. (In Chinese with English Abstract)
17. Zhou, J.X.; Luo, K.; Li, B.; Huang, Z.L.; Yan, Z.F. Geological and isotopic constraints on the origin of the Anle carbonate-hosted Zn-Pb deposit in northwestern Yunnan Province, SW China. *Ore Geol. Rev.* **2016**, *74*, 88–100. [[CrossRef](#)]
18. Zhou, J.X.; Xiang, Z.Z.; Zhou, M.F.; Feng, Y.X.; Luo, K.; Huang, Z.L.; Wu, T. The giant Upper Yangtze Pb-Zn province in SW China: Reviews, new advances and a new genetic model. *J. Asian Earth Sci.* **2018**, *154*, 280–315. [[CrossRef](#)]
19. Zhang, C.Q.; Mao, J.W.; Wu, S.P.; Li, H.M.; Liu, F.; Guo, B.J.; Gao, D.R. Distribution, characteristics and genesis of Mississippi Valley-Type Pb-Zn deposits in Sichuan-Yunnan-Guizhou area. *Miner. Deposits* **2005**, *24*, 336–348. (In Chinese with English Abstract)
20. Tang, Y.Y.; Zhang, K.X.; Tian, Y.J.; Zhang, J.W.; Huang, Z.L.; Wu, T. REE compositions of calcites from Pb-Zn deposits in the eastern Guizhou and their metallogenic implications. *Acta Mineral. Sin.* **2020**, *40*, 356–366. (In Chinese with English Abstract)
21. Elderfield, H.; Upstill-Goddard, R.; Sholkovitz, E.R. The rare earth elements in rivers, estuaries, and coastal seas and their significance to the composition of ocean waters. *Geochim. Cosmochim. Acta* **1990**, *54*, 971–991. [[CrossRef](#)]
22. Johannesson, K.H.; Stetzenbach, K.J.; Hodge, V.F. Rare earth elements as geochemical tracers of regional groundwater mixing. *Geochim. Cosmochim. Acta* **1997**, *61*, 3605–3618. [[CrossRef](#)]
23. Debruyne, D.; Hulsbosch, N.; Muchez, P. Unraveling rare earth element signatures in hydrothermal carbonate minerals using a source-sink system. *Ore Geol. Rev.* **2016**, *72*, 232–252. [[CrossRef](#)]
24. Sun, G.T.; Shen, N.P.; Su, W.C.; Feng, Y.X.; Zhao, J.X.; Peng, J.T.; Dong, W.D.; Zhao, H. Characteristics and Implication of Trace Elements and Sr-Nd Isotope Geochemistry of Calcites from the Miaolong Au-Sb Deposit, Guizhou Province, China. *Acta Mineral Sin.* **2016**, *36*, 404–412. (In Chinese with English Abstract)
25. Zhao, D.; Han, R.S.; Wang, J.S.; Ren, T. REE Geochemical Characteristics in Lehong Large Pb-Zn Deposit, Northeastern Yunnan Province, China. *Acta Mineral. Sin.* **2017**, *37*, 588–595. (In Chinese with English Abstract)

26. Li, X.G.; Yang, K.G.; Hu, X.Y.; Dai, C.G.; Zhang, H. Formation and evolution of the Kaili-Sandu fault in East Guizhou, China. *J. Chengdu Univ. Technol. Sci. Technol. Ed.* **2012**, *39*, 18–26. (In Chinese with English Abstract)
27. Liu, Y.L.; Yang, K.G.; Deng, X. Activities History of Zhenyuan-Guiyang Fault Belts and Constraint on the Evolution of Centre Guizhou Uplift. *Bull. Geol. Sci. Technol.* **2009**, *28*, 41–47. (In Chinese with English Abstract)
28. Deng, X.; Yang, K.G.; Liu, Y.L.; She, Z.B. Characteristics and tectonic evolution of Qianzhong Uplift. *Earth Sci. Front.* **2010**, *17*, 79–89. (In Chinese with English Abstract)
29. Yang, K.G.; Li, X.G.; Dai, C.G.; Zhang, H.; Zhou, Q. Analysis of the origin of trough-like folds in Southeast Guizhou. *Earth Sci. Front.* **2012**, *19*, 53–60. (In Chinese with English Abstract)
30. Dai, C.G.; Wang, M.; Chen, J.S.; Wang, X.H. Tectonic Movement Characteristic and Its Geological Significance of Guizhou. *Guizhou Geol.* **2013**, *30*, 119–124. (In Chinese with English Abstract)
31. Ye, L.; Liu, T.G.; Shao, S.X. Geochemistry of mineralizing fluid of Cd-rich zinc deposit: Taking Niujiatong Cd-rich zinc deposit, Duyun, Guizhou for example. *Geochimica* **2000**, *29*, 597–603. (In Chinese with English Abstract)
32. Zhao, Z.; Bao, G.P.; Qian, Z.K.; Huang, L.; Lu, M.D.; Xu, L. Geochemical Characteristics of C-O Isotopes and REE in the Hydrothermal Calcite from the Shuanglongquan Pb-Zn Deposit, Southern Guizhou, China. *Acta Mineral. Sin.* **2018**, *38*, 627–636. (In Chinese with English Abstract)
33. Cui, M.; Tang, L.J.; Guo, T.L.; Ning, F.; Tian, H.Q.; Hu, D.F. Structural Style and Thrust Breakthrough Model of Fold in Southeast Guizhou. *Earth Sci. (Wuhan China)* **2009**, *34*, 907–913. (In Chinese with English Abstract)
34. Dai, C.G.; Chen, J.S.; Lu, D.B.; Ma, H.Z.; Wang, X.H. Appearance and geologic significance of Caledonian Movement in southeastern Guizhou, China and its adjacent area. *Geol. Bull. China* **2010**, *29*, 530–534. (In Chinese with English Abstract)
35. Xu, Z.Y.; Yao, G.S.; Guo, Q.X.; Chen, Z.L.; Dong, Y.; Wang, P.W.; Ma, L.Q. Genetic Interpretation about Geotectonics and Structural Transfiguration of the Southern Guizhou Depression. *Geotecton. Metallog.* **2010**, *34*, 20–31. (In Chinese with English Abstract)
36. Luo, K.; Zhou, J.X.; Huang, Z.L.; Caulfield, J.; Zhao, J.X.; Feng, Y.X.; Ouyang, H. New insights into the evolution of Mississippi Valley-Type hydrothermal system: A case study of the Wusihe Pb-Zn deposit, South China, using quartz in-situ trace elements and sulfides in situ S-Pb isotopes. *Am. Mineral.* **2020**, *105*, 35–51. [[CrossRef](#)]
37. Zhou, J.X.; Meng, Q.T.; Ren, H.Z.; Sun, G.T.; Zhang, Z.J.; An, Q.; Zhou, C.X. A super-large co-(associative) Ge deposit was discovered in the Huangsi anticline area of Guizhou. *Geotecton. Metallog.* **2020**, *44*, 1025–1026. (In Chinese with English Abstract)
38. Zuo, J.L. Geological characteristics and ore-controlling factors of the Banbianjie Pb-Zn deposit in Guiding County, Guizhou Province. *Land Resour. South. China* **2013**, *5*, 39–41. (In Chinese)
39. Mo, L.L. Geological Characteristics and Origin of Banbianjie Zinc Deposit in Guiding County, Guizhou Province. *West-China Explor. Eng.* **2020**, *32*, 125–127+132. (In Chinese with English Abstract)
40. Qi, L.; Hu, J.; Gregoire, D.C. Determination of trace elements in granites by inductively coupled plasma mass spectrometry. *Talanta* **2000**, *51*, 507–513.
41. Raczek, I.; Stoll, B.; Hofmann, A.W.; Jochum, K.P. High-Precision Trace Element Data for the USGS Reference Materials BCR-1, BCR-2, BHVO-1, BHVO-2, AGV-1, AGV-2, DTS-1, DTS-2, GSP-1 and GSP-2 by ID-TIMS and MIC-SSMS. *Geostand. Newsl.* **2001**, *25*, 77–86. [[CrossRef](#)]
42. Cotta, A.J.B.; Enzweiler, J. Classical and new procedures of whole rock dissolution for trace element determination by ICP-MS. *Geostand. Geoanal. Res.* **2012**, *36*, 27–50. [[CrossRef](#)]
43. Chen, D.F.; Huang, Y.Y.; Yuan, X.L.; Cathles, L.M. Seep carbonates and preserved methane oxidizing archaea and sulfate reducing bacteria fossils suggest recent gas venting on the seafloor in the Northeastern South China Sea. *Mar. Petrol. Geol.* **2005**, *22*, 613–621. [[CrossRef](#)]
44. Chen, L.; Liu, Y.S.; Hu, Z.C.; Gao, S.; Zong, K.Q.; Chen, H.H. Accurate determinations of fifty-four major and trace elements in carbonate by LA-ICP-MS using normalization strategy of bulk components as 100%. *Chem. Geol.* **2011**, *284*, 283–295. [[CrossRef](#)]
45. Jochum, K.P.; Weis, U.; Stoll, B.; Kuzmin, D.; Yang, Q.C.; Raczek, I.; Jacob, D.; Stracke, A.; Birbaum, K.; Frick, D.A.; et al. Determination of reference values for NIST SRM 610-617 glasses following ISO guidelines. *Geostand. Geoanal. Res.* **2011**, *35*, 397–429. [[CrossRef](#)]
46. Jochum, K.P.; Scholz, D.; Stoll, B.; Weis, U.; Wilson, S.A.; Yang, Q.Y.; Schwalb, A.; Börner, N.; Jacob, D.E.; Andreae, M.O. Accurate trace element analysis of speleothems and biogenic calcium carbonates by LA-ICP-MS. *Chem. Geol.* **2012**, *318*, 31–44. [[CrossRef](#)]
47. Boynton, W.V. *Cosmochemistry of the Rare Earth Elements: Meteorite Studies Developments in Geochemistry*; Elsevier: Amsterdam, The Netherlands, 1984; pp. 63–114.
48. Yan, M.C.; Chi, Q.H. *Geochemical Composition of Crust and Rocks in Eastern China*; Science Press: Beijing, China, 1997; pp. 1–292. (In Chinese)
49. Gao, J.B.; Yang, R.D.; Tao, P.; Cheng, W.; Zheng, L.L. Study on the Genesis of Devonian Magnesian Siderite Deposits in the Northwestern Guizhou Province. *Geol. Rev.* **2015**, *61*, 1305–1320. (In Chinese with English Abstract)
50. Shannon, R.D. Revised effective ionic radii and systematic studies of interatomic distances in halides and chalcogenides. *Acta Crystallogr. A* **1976**, *32*, 751–767. [[CrossRef](#)]
51. Liu, Y.J.; Cao, L.M.; Li, Z.L. *Elemental Geochemistry*; Science Press: Beijing, China, 1984; pp. 360–420. (In Chinese)
52. Tang, Y.Y.; Bi, X.W.; He, L.P.; Wu, L.Y.; Feng, C.X.; Zou, Z.C.; Tao, Y.; Hu, R.Z. Geochemical characteristics of trace elements, fluid inclusions and carbon-oxygen isotopes of calcites in the Jinding Zn-Pb deposit, Lanping, China. *Acta Petrol. Sin.* **2011**, *27*, 2635–2645. (In Chinese with English Abstract)

53. Leach, D.L.; Sangster, D.F.; Kelley, K.D.; Ross, R.L.; Garven, G.; Allen, C.R.; Gutzmer, J.; Walters, S. Sediment-hosted lead-zinc deposits: A global perspective. *Econ. Geol.* **2005**, *100*, 561–607.
54. Yang, Q.K.; Meng, X.J.; Guo, F.S.; Zhou, W.P.; Sun, Q.Z. Characteristics of Trace Elements in Gangue Minerals of the Xiangshan Uranium Polymetallic Deposit, Jiangxi, and its Geological Significance. *Bull. Mineral. Petrol. Geochem.* **2014**, *33*, 457–465+483. (In Chinese with English Abstract)
55. Michard, A. Rare earth element systematics in hydrothermal fluids. *Geochim. Cosmochim. Acta* **1989**, *53*, 745–750. [[CrossRef](#)]
56. Lottermoser, B.G. Rare earth elements and hydrothermal ore formation processes. *Ore Geol. Rev.* **1992**, *7*, 25–41. [[CrossRef](#)]
57. Bau, M.; Dulski, P. Comparing yttrium and rare earths in hydrothermal fluids from the Mid-Atlantic Ridge: Implications for Y and REE behavior during near-vent mixing and for the Y/Ho ratio of Proterozoic seawater. *Chem. Geol.* **1999**, *155*, 77–90. [[CrossRef](#)]
58. Wang, G.Z.; Hu, R.Z.; Liu, Y.; Sun, G.S.; Sun, W.C.; Liu, H. REE Geochemical Characteristic from Fluorite in Qinglong Antimony Deposit, South-Western Guizhou. *J. Mineral. Petrol.* **2003**, *23*, 62–65. (In Chinese with English Abstract)
59. Zhang, Y.; Xia, Y.; Wang, Z.P.; Yan, B.W.; Fu, Z.K.; Chen, M. REE and stable isotope geochemical characteristics of Bojitian gold deposit, Guizhou Province. *Earth Sci. Front.* **2010**, *17*, 385–395. (In Chinese with English Abstract)
60. Zhou, J.X.; Huang, Z.L.; Zhou, G.F.; Li, X.B.; Ding, W.; Bao, G.P. The trace elements and rare earth elements geochemistry of sulfide minerals of the Tianqiao Pb-Zn ore deposit, Guizhou Province, China. *Acta Geol. Sin.* **2011**, *85*, 189–199.
61. Möller, P.; Parekh, P.P.; Schneider, H.J. The application of Tb/Ca-Tb/La abundance ratios to problems of fluorite genesis. *Miner. Deposita* **1976**, *11*, 111–116. [[CrossRef](#)]
62. Bau, M.; Dulski, P. Comparative study of yttrium and rare-earth element behaviors in fluorine-rich hydrothermal fluids. *Contrib. Mineral. Petr.* **1995**, *119*, 213–223. [[CrossRef](#)]
63. Li, H.M.; Shen, Y.C.; Mao, J.W.; Liu, T.B.; Zhu, H.P. REE features of quartz and pyrite and their fluid inclusions: An example of Jiaojia-type gold deposits, northwestern Jiaodong peninsula. *Acta Petrol. Sin.* **2003**, *19*, 267–274. (In Chinese with English Abstract)
64. Wei, H.T.; Shao, Y.J.; Ye, Z.; Xiong, Y.Q.; Zhou, H.D.; Xie, Y.L. REE and Sr isotope geochemistry of gangue calcites from Huayuan Pb-Zn orefield in western Hunan, China. *Chin. J. Nonferrous Met.* **2017**, *27*, 2329–2339. (In Chinese with English Abstract)
65. Liu, S.W.; Shi, S.; Li, R.X.; Gao, Y.B.; Liu, L.F.; Duan, L.Z.; Chen, B.Z.; Zhang, S.N. REE geochemistry of Mayuan Pb-Zn deposit on northern margin of Yangtze Plate. *Miner. Deposits* **2013**, *32*, 979–988. (In Chinese with English Abstract)
66. Chen, Y.J.; Fu, S.G. Variation of REE patterns in early Precambrian sediments: Theoretical study and evidence from the southern margin of the northern China craton. *Chin. Sci. Bull.* **1991**, *36*, 1100–1104.
67. Chen, Y.J.; Zhao, Y.C. Geochemical characteristics and evolution of REE in the Early Precambrian sediments: Evidences from the southern margin of the North China craton. *Episodes J. Int Geosci.* **1997**, *20*, 109–116.
68. Ma, Y.J.; Liu, C.Q. Trace element geochemistry during weathering as exemplified by the weathered crust of granite, Longnan, Jiangxi. *Sci. Bull.* **1999**, *44*, 2260–2263. [[CrossRef](#)]
69. Rimstidt, J.D.; Balog, A.; Webb, J. Distribution of trace elements between carbonate minerals and aqueous solutions. *Geochim. Cosmochim. Acta* **1998**, *62*, 1851–1863. [[CrossRef](#)]
70. Bau, M.; Möller, P. Rare earth element fractionation in meta-morphogenic hydrothermal calcite, magnesite and siderite. *Miner. Petrol.* **1992**, *45*, 231–246. [[CrossRef](#)]
71. He, S.; Xia, Y.; Xiao, J.; Gregory, D.; Xie, Z.J.; Tan, Q.P.; Yang, H.Y.; Guo, H.Y.; Wu, S.W.; Gong, X.X. Geochemistry of REY-Enriched Phosphorites in Zhijin Region, Guizhou Province, SW China: Insight into the Origin of REY. *Minerals* **2022**, *12*, 408. [[CrossRef](#)]
72. Cherniak, D.J.; Zhang, X.Y.; Wayne, N.K.; Watson, E.B. Sr, Y and REE diffusion in fluorite. *Chem. Geol.* **2001**, *181*, 99–111. [[CrossRef](#)]
73. Bau, M. Rare-earth element mobility during hydrothermal and metamorphic fluid-rock interaction and the significance of the oxidation state of europium. *Chem. Geol.* **1991**, *93*, 219–230. [[CrossRef](#)]
74. Cocherie, A.; Calvez, J.Y.; Oudin-Dunlop, E. Hydrothermal activity as recorded by Red Sea sediments: Sr-Nd isotopes and REE signatures. *Mar. Geol.* **1994**, *118*, 291–302. [[CrossRef](#)]
75. Mills, R.A.; Elderfield, H. Rare earth element geochemistry of hydrothermal deposits from the active TAG Mound, 26°N Mid-Atlantic Ridge. *Geochim. Cosmochim. Acta* **1995**, *59*, 3511–3524. [[CrossRef](#)]
76. Zhong, S.; Mucci, A. Partitioning of rare earth elements (REEs) between calcite and seawater solutions at 25°C and 1 atm, and high dissolved REE concentrations. *Geochim. Cosmochim. Acta* **1995**, *59*, 443–453. [[CrossRef](#)]
77. Peng, J.T.; Hu, R.Z.; Qi, L.; Zhao, J.H.; Fu, Y.Z. REE Distribution Pattern for the Hydrothermal Calcites from the Xikuangshan Antimony Deposit and Its Constraining Factors. *Geol. Rev.* **2004**, *50*, 25–32. (In Chinese with English Abstract)
78. Murowchick, J.B.; Barnes, H.L. Marcasite precipitation from hydrothermal solutions. *Geochim. Cosmochim. Acta* **1986**, *50*, 2615–2629. [[CrossRef](#)]
79. Wang, M.Y.; Xi, C.Z.; Li, Y. 2008. Geological and geochemical characteristics of the barite rocks in the hydrothermal sedimentary deposit in Guangxi. *Min. Resour. Geol.* **2008**, *22*, 335–341. (In Chinese with English Abstract)
80. Niu, H.C.; Chen, F.R.; Lin, M.Q. REE Geochemistry of Magmatic genetic Barite and Fluorite. *Acta Mineral. Sin.* **1996**, *16*, 328–388. (In Chinese with English Abstract)

81. Yang, D.Z.; Zhou, J.X.; Luo, K.; Yu, J.; Zhou, Z.H. New discovery and research value of Zhulingou zinc deposit in Guiding, Guizhou. *Bull. Mineral. Petrol. Geochem.* **2020**, *39*, 344–345. (In Chinese with English Abstract)
82. Zhou, J.X.; Wang, X.C.; Wilde, S.A.; Luo, K.; Huang, Z.L.; Wu, T.; Jin, Z.G. New insights into the metallogeny of MVT Zn-Pb deposits: A case study from the Nayongzhi in South China, using field data, fluid compositions, and in situ S-Pb isotopes. *Am. Mineral.* **2018**, *103*, 91–108. [[CrossRef](#)]

**Disclaimer/Publisher’s Note:** The statements, opinions and data contained in all publications are solely those of the individual author(s) and contributor(s) and not of MDPI and/or the editor(s). MDPI and/or the editor(s) disclaim responsibility for any injury to people or property resulting from any ideas, methods, instructions or products referred to in the content.